

Transformer based Fingerprint Feature Extraction

Saraansh Tandon

International Institute of Information and Technology,
Hyderabad, India 500032

Email: saraansh.tandon@research.iiit.ac.in

Anoop Namboodiri

International Institute of Information and Technology,
Hyderabad, India 500032

Email: anoop@iiit.ac.in

Abstract—Fingerprint feature extraction is a task that is solved using either a global or a local representation. State-of-the-art global approaches use heavy deep learning models to process the full fingerprint image at once, which makes the corresponding approach memory intensive. On the other hand, local approaches involve minutiae based patch extraction, multiple feature extraction steps and an expensive matching stage, which make the corresponding approach time intensive. However, both these approaches provide useful and sometimes exclusive insights for solving the problem. Using both approaches together for extracting fingerprint representations is semantically useful but quite inefficient. Our convolutional transformer based approach with an in-built minutiae extractor provides a time and memory efficient solution to extract a global as well as a local representation of the fingerprint. The use of these representations along with a smart matching process gives us state-of-the-art performance across multiple databases. The project page can be found at <https://saraansh1999.github.io/global-plus-local-fp-transformer>.

I. INTRODUCTION

From daily usage in smartphones to granting access to highly confidential resources, fingerprints have proven to be a reliable source of biometric identity. Hence it comes as no surprise that this field has been a very active domain of research since many decades. Most fingerprint feature extraction algorithms today are built upon the domain knowledge of global features like ridge-flow or local features like minutiae and pores. Knowledge of at least one of these, possibly in combination with others, is used to process an input fingerprint image and output a representation. This representation acts as a proxy of the image and is used to determine the identity of the owner of the fingerprint by matching it with a database.

Global approaches for extracting fixed-length fingerprint representations function by processing the full image as shown in Figure 2a. One of the first such attempts was made by Jain et al. in Fingercode [1] where a set of Gabor filters were used to produce a 640 byte long representation. Later as the deep learning era emerged, [2] and [3] made use of convolutional networks for the same. Recently, Engelsma et al. proposed DeepPrint[4] which uses a multi-task approach to incorporate domain knowledge into deep learning of fingerprint representations and obtains state-of-the-art performance among fixed-length global approaches.

Local approaches function by breaking down the input image into multiple local patches based on some local features. The most popular of these local features of interest are the minutiae points, because of their studied permanence [5] and uniqueness [6] among humans. [7], [8], and [9] proposed methods that led

to fixed-length representations, but local approaches may also lead to variable-length representations whose size depends on the number of minutiae identified in the input image. Cao et al. proposed such an end-to-end method called LatentAFIS[10] as shown in Figure 2b. It treats the entire set of the predicted minutiae and their corresponding embeddings as the representation of the full fingerprint.

Since DeepPrint[4] and LatentAFIS[10] obtain state-of-the-art performances in their respective domains, we treat them as baselines for our approach. On analyzing the mutually exclusive failure cases of [4] and [10] we observe that the global and local perspectives can compensate for the semantic shortcomings of each other. Figure 1a shows a pair of fingerprints originating from two different identities, but due to a similar ridge-flow structure, [4] marks it as a true pair. Whereas [10] is able to focus on the subtle differences existing in the minutiae and mark it accurately as a false pair. Figure 1b shows a pair of impressions from the same finger, but [11] claims that distortion is able to fool [10] which misses a lot of minutiae matches as the corresponding patches look significantly different. [4] on the other hand is able to look at the big picture similarities at the center of the fingerprint to make the correct prediction. Note that [4] is inferior in overall performance as compared to [10] as the latter is much more strongly tied to the domain knowledge of fingerprints.

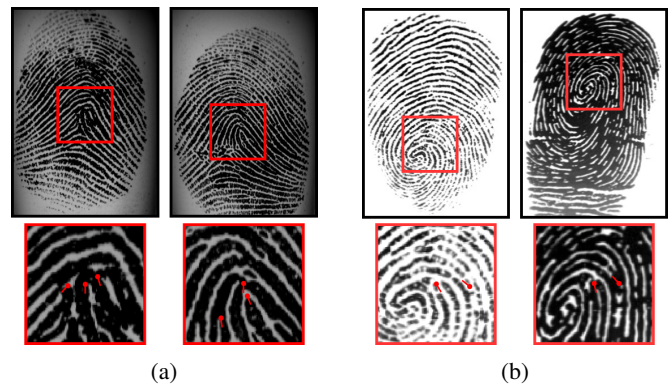


Fig. 1: Mutually exclusive failure cases of [4] and [10] respectively where the other method works well.

Hence we posit that using both global and local approaches together can help eliminate a lot of failure cases and consequently boost performance. But a naive combination poses issues including: 1) Slow feature extraction of [10] due to

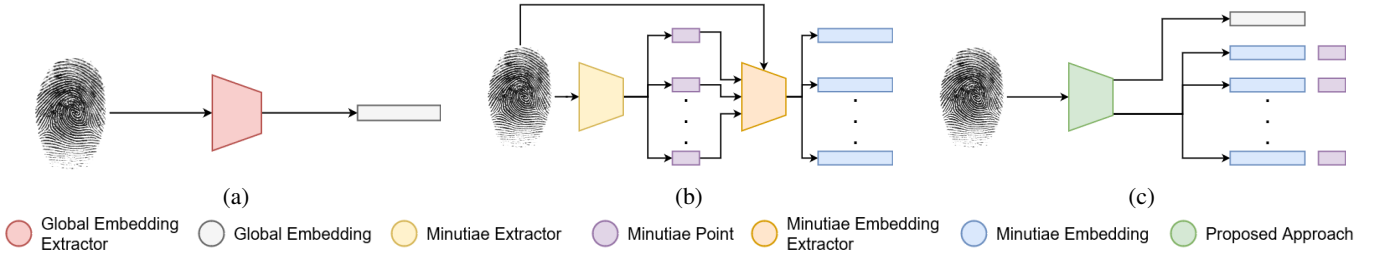


Fig. 2: Approaches for Fingerprint representation extraction: (a) A global approach that outputs a fixed-length representation. (b) A local approach that first extracts a variable number of minutiae points and then extracts representations corresponding to each of them. (c) Proposed methodology extracts a global fixed length representation, minutiae points and representations corresponding to all minutiae points in an end-to-end fashion.

expensive minutiae detection and multiple feature extraction steps. 2) Huge memory consumption of [4] due to use of big models. 3) Expensive graph matching of [10] as it evaluates all possible minutiae pairs between two images.

To facilitate the semantic fusion of global and local approaches while avoiding any of the aforementioned issues, we propose a novel methodology as shown in Figure 2c. We can list out the contributions of our paper as:

- A novel architecture which, provided a fingerprint image, can in a single forward pass generate: 1) a global representation 2) a set of minutiae points 3) a local representation for each of the predicted minutiae points. Whereas other state-of-the-art methods usually use a separate model for each of those steps.
- A methodology that:
 - is 57.93% smaller in size than [4].
 - does 54.41% faster feature extraction and 78.47% faster feature matching as compared to [10]
 - obtains a state-of-the-art $FRR = \%@FAR = 0.1\%$ of 1.45 over 6 standard matching databases as compared to 5.65 of [4] and 2.32 of [10].
- First work to the best of our knowledge which makes use of a transformer model for fingerprint feature extraction.

Our approach makes use of a Convolutional Transformer based architecture because 1) the image classification capability of transformer models, as demonstrated in [12], make them suitable for global feature extraction. 2) the ability of transformers to deal with sequences and object localisation, as demonstrated in [13], make them suitable for multiple local feature extraction. 3) it has been shown by [2], [4], [8], [9] [10] that convolutional networks are effective in fingerprint representation extraction. 4) the utility of transformers for dealing with fingerprint images has been shown in [14].

II. METHODOLOGY

We will first describe the architecture of the model used in our approach, followed by details of training and inference.

A. Architecture

We use an encoder-decoder style architecture, as shown in Figure 3, to “translate” an input fingerprint image into the required representations. Let the input be a fingerprint image

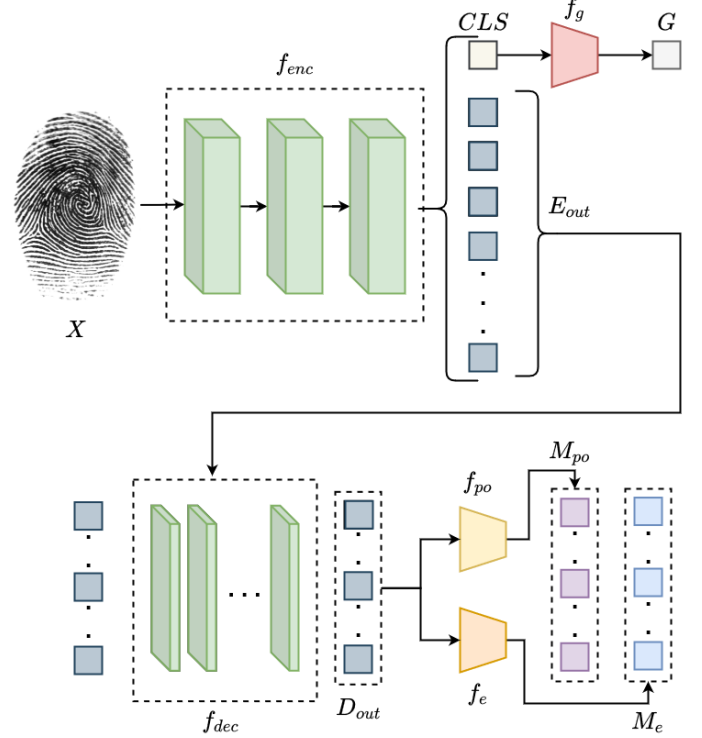


Fig. 3: Architecture of the encoder-decoder style model (f_{model}) used in our methodology.

$X \subseteq R^{C \times H \times W}$ where C is the number of channels and H, W represent the size of the image.

1) *Encoder*: We use a CvT-13 [15] model f_{enc} as our encoder which consists of 3 stages of Convolutional Transformer Blocks. On passing X through f_{enc} we obtain a $CLS \subseteq R^{d_{enc}}$ token along with $E_{out} \subseteq R^{L_{enc} \times d_{enc}}$ which is a sequence of L_{enc} embeddings of size d_{enc} . Similar to traditional classification tasks we employ the CLS token to capture a global essence of the input and hence it is passed through a linear layer f_g to produce the final global representation of our approach $G \subseteq R^{d_g}$ where d_g is the dimensionality of said representation. E_{out} tokens are usually ignored for classification tasks, but similar to [16], [17] we posit that these tokens can be used to extract useful auxiliary information about the input. Hence these tokens act as a “summary” of the input image and are passed on to the decoder as its “memory” input.

2) *Decoder*: We design a 6 layer decoder f_{dec} where we consider E_{out} as the “memory” input and use a placeholder “target” sequence of length L similar to the object queries defined by [13]. f_{dec} computes token embeddings $D_{out} \subseteq R^{L \times d_{dec}}$ where d_{dec} refers to the dimensionality of the decoder. Each of the L tokens of D_{out} is representative of one minutia of the fingerprint and hence D_{out} is passed through:

- Pos-Ori MLP (f_{po}): This 3 layer MLP outputs $M_{po} \subseteq R^{L \times 3}$ which represents the 2D coordinates and orientation of the L minutiae points predicted in the image.
- MinEmb MLP (f_e): This 1 layer MLP outputs $M_e \subseteq R^{L \times d_m}$ which is the local representation of the L minutiae points of the image as characterized by M_{po} . Here d_m represents the dimensionality of the local minutiae representations.

Together M_{po} and M_e form the final local representation of the input fingerprint. Here L is a hyperparameter determined by the average number of minutiae in the training data.

Algorithm 1 Forward pass of the proposed model. (f_{model})

Input: $X \subseteq R^{C \times H \times W}$

Output: G, M_{po}, M_e

- 1: $CLS, E_{out} \leftarrow f_{enc}(X)$
 - 2: $G \leftarrow f_g(CLS)$
 - 3: $D_{out} \leftarrow f_{dec}(E_{out})$
 - 4: $M_{po} \leftarrow f_{po}(D_{out})$
 - 5: $M_e \leftarrow f_e(D_{out})$
-

B. Training Stage

We pass the input through the model as described in Algorithm 1 and train using a multi-task learning framework so as to facilitate the learning of both global and local perspectives. Global Loss L_g adopts a teacher-student framework for training the model to generate good global representations for fingerprints. We use [4] as our teacher model and use it to generate ground truth embeddings ($G' \subseteq R^{192}$) for our training images.

$$L_g = MSE(G, G') \quad (1)$$

We use a COTS minutiae extractor called Verifinger to generate ground truth locations and orientations ($M'_{po} \subseteq R^{L \times 3}$) of minutiae points for each image in our training dataset. Since our model predicts a fixed number (L) of minutiae per image, we pick the top L candidates based on confidence scores. Next, we obtain the ground truth of the local representations corresponding to the minutiae in M'_{po} similar to [11]. This gives us ground truth local representations $M'_e \subseteq R^{L \times 64}$.

To establish correspondences between the predicted and ground truth minutiae points in an image (Figure 4), we make use of a Hungarian matcher[18] that scores each correspondence using a linear combination of the L2 distances between the minutiae locations, orientations and representations. Once these correspondences are predicted, we reorder M'_{po} and M'_e to M''_{po} and M''_e respectively and use:

$$L_{po} = MSE(M_{po}, M''_{po}) \quad (2)$$

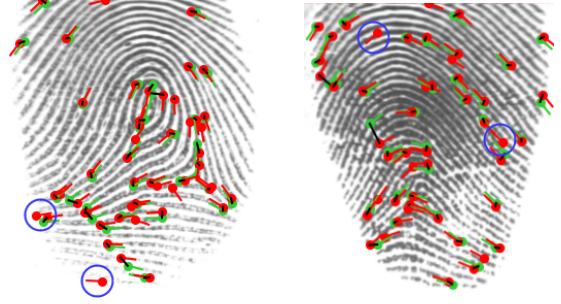


Fig. 4: Green represents the ground truth Verifinger minutiae, whereas red represents the minutiae predicted by our model. Black lines represents the correspondences established by the Hungarian Matcher[18]. Blue represents spurious minutiae.

$$L_e = MSE(M_e, M''_e) \quad (3)$$

We also include supervision over the outputs of the intermediate layers of the decoder. For this we use Eqn. 4 and 5 where M_{po_i} and M_{e_i} are the outputs of f_{po} and f_e respectively, when applied on the output of the decoder’s i^{th} layer. M''_{po_i} and M''_{e_i} are the re-orderings of the ground truths (M'_{po} and M'_e) based on Hungarian matching with M_{po_i} and M_{e_i} .

$$L_{po}^{inter} = \sum_{i=1}^5 MSE(M_{po_i}, M''_{po_i}) \quad (4)$$

$$L_e^{inter} = \sum_{i=1}^5 MSE(M_{e_i}, M''_{e_i}) \quad (5)$$

Overall this multi-task, teacher-student training paradigm is guided using the following loss function:

$$L_{tot} = \lambda_g L_g + \lambda_{po} L_{po} + \lambda_e L_e + \lambda_{po}^{inter} L_{po}^{inter} + \lambda_e^{inter} L_e^{inter} \quad (6)$$

C. Inference Algorithm

Given two images, the inference process of our approach has multiple steps as shown in Algorithm 2.

Feature extraction stage is executed in steps 1 and 2 which simply includes running the forward pass of the model.

Global Matching (step 3) stage involves a dot product between G_a and G_b as they are fixed-length global representations.

Although our transformer based approach is able to parallelly extract global and local feature representations, to reap the benefits of all that information we need to perform global and local matching both. Due to the expensive nature of minutiae matchers (*MinMatch*), this will lead to an inefficient inference algorithm. To counter this we introduce a **Thresholding** stage which determines the cases where local matching is not expected to add significant value to the approach. Since the calculation of s_g is pretty fast, Thresholding uses it to filter out the cases where solely the global representation leads to a confident inference. Specifically, step 4 represents a highly confident genuine pair prediction and step 6 represents a highly confident impostor pair prediction. In such cases we only use

Algorithm 2 Inference using proposed methodology.

Input: $X_a, X_b \subseteq R^{C \times H \times W}$ **Output:** s

- 1: $G_a, M_{poa}, M_{ea} \leftarrow f_{model}(X_a)$
 - 2: $G_b, M_{pob}, M_{eb} \leftarrow f_{model}(X_b)$
 - 3: $s_g \leftarrow Norm(G_a \bullet G_b)$ ▷ Global matching score
 - 4: **if** $s_g > \theta_t$ **then**
 - 5: $s_l \leftarrow 1$
 - 6: **else if** $s_g < \theta_f$ **then**
 - 7: $s_l \leftarrow 0$
 - 8: **else**
 - 9: $s_l \leftarrow Norm(MinMatch(M_{poa}, M_{ea}, M_{pob}, M_{eb}))$
 - 10: ▷ Local matching score
 - 11: **end if**
 - 12: $s \leftarrow (s_g + s_l)/2$ ▷ Final matching score
-

s_g to make the final inference by assigning trivial constants to s_l (steps 5 and 7).

On the other hand if $\theta_f \leq s_g \leq \theta_t$, we assume that the global representation is not good enough for inference and hence only in these cases Thresholding permits the execution of **Local Matching** to obtain s_l (step 9).

Dot products used for Global Matching produce scores in the range $[0, 1]$, whereas *MinMatch* used of Local Matching produces unbounded scores greater than 0 (sum of cosine similarities of all the matched minutiae). On combining the raw scores, local matching will dominate and any possible advantages of the global perspective would fade out. Therefore, before combining these scores we need to align their distributions using a **Score Normalization** function (*Norm*). We make use of the *Double Sigmoid*[19] for this purpose as it is able to bring both distributions in the range $[0, 1]$ while being robust and highly efficient[20].

The final scores are obtained using **Mean-Fusion** (step 12) to combine the normalized scores. Other score normalization and fusion approaches have been explored in Section V-C.

Any inference hyperparameters can be obtained using a hold-out dataset readily available in most real-world scenarios. Score distributions across various steps when Algorithm 2 is operated on all pairs of a dataset are shown in Figure 5. The utility of fusion is clearly represented by the reduced overlapping regions in Figure 5d as compared to those in Figure 5a.

III. DATASETS

For training and validation purposes we have used an in-house dataset made up of fingerprint images captured using CrossMatch and DigitalPersona optical sensors. The training and validation splits consist of 130K and 38K images respectively. For evaluation of fingerprint matching we report on different sensors of FVC 2000 [21], FVC 2002 [22], FVC 2004 [23] and FVC 2006 [24] datasets following the official protocols. Each sensor of the FVC 2000, 2002 and 2004 datasets contains 100 subjects with 8 impressions per subject, leading to 2800 genuine ($= 100 \times {}^8C_2$) and 4950 impostor ($= {}^{100}C_2$) comparisons, while each sensor within the FVC

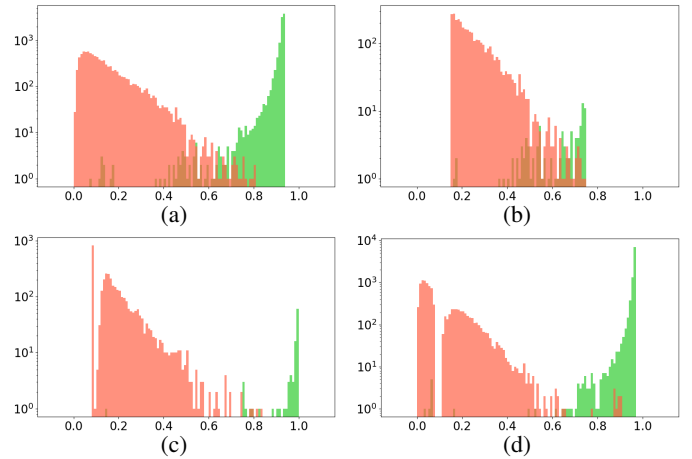


Fig. 5: Red color represents scores of impostor pairs and green represents scores of genuine pairs. (a) Global Matching Scores for all pairs. (b) Global Matching Scores corresponding to cases where Thresholding permits Local Matching ($\theta_t = 0.75, \theta_f = 0.15$). (c) Local Matching Scores corresponding to cases where Thresholding permits Local Matching. (d) Final Matching Scores for all pairs.

2006 dataset contains 140 subjects with 12 impressions per subject leading to 9240 ($= 140 \times {}^{12}C_2$) genuine and 9730 ($= {}^{140}C_2$) impostor comparisons.

IV. EXPERIMENTS AND RESULTS

We compare our proposed methodology with [4] and [10] as they are the current state-of-the-art approaches for global and local matching respectively. We also compare with the performance obtained by using a straightforward combination of [4] and [10] called **Cascade**. In this, feature extraction and matching are performed by running both approaches independently to completion and fusing the final matching scores as described in Algorithm 2. This is done to provide insight into how our methodology helps in parallelizing aspects of global and local approaches. We do not make comparisons with commercial matchers like VeriFinger as their proprietary nature prevents the evaluation of their complexity and we want to focus on generating an efficient approach.

Since we train using a private dataset, to make our work reproducible we present the experimentation and details of a model trained using public datasets in the supplementary.

A. Matching

Since our training dataset consists of optical images, in this experiment we evaluate on the various optical sensors of FVC datasets to assess the same-sensor performance of our approach. The minutiae predicted by our methodology obtain a Goodness Index and average positional error[25] of 0.31 and 5.51 pixels respectively (with a distance threshold of 20 pixels) which is comparable to 0.20 and 5.29 pixels obtained by the open source minutiae extractor [26]. This indicates the utility of our approach for the task of minutiae detection.

In Table I we report the metric $FRR\%@FAR = 0.1\%$ and

TABLE I: Comparison of the matching performance ($FRR\%@FAR = 0.1\%$) on FVC datasets’ optical sensors

Method	2006		2004		2002		2000		Average [†]
	DB2A	DB1A	DB2A	DB1A	DB2A	DB1A	DB3A		
DeepPrint [4]	0.30	3.86	9.96	7.25	3.75	3.96	5.14	5.65	
LatentAFIS [10]	0.00	5.54	4.02	0.79	0.36	1.39	1.79	2.32	
Cascade	<u>0.01</u>	<u>3.39</u>	2.62	1.65	0.93	<u>1.32</u>	<u>1.50</u>	<u>1.90</u>	
Our	0.12	2.00	<u>2.73</u>	<u>1.11</u>	<u>0.86</u>	1.04	0.93	1.45	

Best and second best results are in bold and underline respectively.

[†] FVC 2006 DB2A has not been included in the average as it is used as a hold-out dataset in Sections V-B and V-C.

the ROC curves for [23] can be found in the supplementary. Our methodology clearly beats both of the current state-of-the-art methods on 4 and the Cascade baseline on 5 datasets individually. Moreover we beat all three baselines on an average of 6 datasets. Hence this proves the state-of-the-art nature of our approach for the task of matching.

B. Time and Memory

We can observe in Figure 6a that our method is 54.41% faster than [10] and has almost the same speed as [4] in the feature extraction stage. This leads to a 68.72% speed-up as compared to Cascade for the same.

Figure 6b shows that our method achieves a significant speed-up in the feature matching stage as compared to [10] which leads to a 78.88% speed-up as compared to Cascade.

Finally, Figure 6c shows that our model is 57.93% smaller than the model used in [4], which is a significant advantage to compensate for the difference in matching time of the two approaches. Moreover, it leads to 61.05% more memory efficiency as compared to Cascade. Although we show that our model contains more parameters than [10], it is important to note that here we have excluded the parameters required by [10] to extract minutiae during inference. Verifinger, a black-box operator, is used for that purpose and hence its complexity cannot be evaluated. Whereas our model includes an in-built minutiae detector.

This shows that our methodology is able to bring together the semantic advantages of the two state-of-the-art approaches more efficiently than Cascade by improving upon the bottleneck factors including the time taken by [10] and the memory consumption of [4].

C. Generalization

To evaluate the cross-sensor generalization performance of our approach we evaluate on the non-optical sensors of FVC datasets as shown in Table II. Note that our training data consists of only optical images and hence thermal, synthetic and capacitive sensors are unseen domains for our model. We observe that our approach is able to obtain state-of-the-art performance across three sensors belonging to different domains.

V. ABLATION STUDY

A. Loss function

In this study we try to play around with the supervision provided to train the model by changing the values of the

TABLE II: Comparison of the matching performance ($FRR\%@FAR = 1.0\%$) on FVC datasets’ non-optical sensors

Method	Thermal	Synthetic	Capacitive	Average
	2006DB3A	2006DB4A	2000DB2A	
DeepPrint[4]	5.17	14.58	1.14	6.96
LatentAfis[10]	1.20	2.42	0.14	1.25
Cascade	1.01	1.63	0.11	0.92
Our	1.27	1.18	0.11	0.85

hyperparameters in Eqn. 6 and observe the differences in performance on FVC 2004 DB1A[23]. The magnitude of these hyperparameters was chosen based on the magnitude of loss values on the validation set.

It is clear that a model trained with a combination of local and global supervision is superior to a model trained solely for one of them. Moreover we also observe a significant benefit of including the intermediate loss terms.

TABLE III: $FRR\%@FAR = 0.1\%$ for FVC 2004 DB1A[23] using various loss functions.

λ_g	λ_{po}	λ_e	λ_{po}^{inter}	λ_e^{inter}	$FRR\%$
1	0	0	0	0	5.32
0	1	1	0	0	6.89
10	1	1	0	0	2.79
60	1	1	1	1	2.00

B. Inference parameters

In Algorithm 2 we have made use of θ_t and θ_f for Thresholding. In practice, their values can be obtained using some hold-out representative dataset. Here we make use of the FVC 2006 DB2A[24] dataset to experiment with different combinations of values for these hyperparameters.

Our methodology retains all of its utility except for feature matching speed-up when trivial constants are used for θ_t and θ_f . Such a case is shown in the first row of Table IV. Subsequently we observe that as the gap between θ_t and θ_f decreases, the matching time decreases too, as the number of cases for which Thresholding permits local matching decreases. But after a while it leads to a decrease in performance as the advantage of fusing local scores with global ones fades out. For our results presented in Section IV we have used

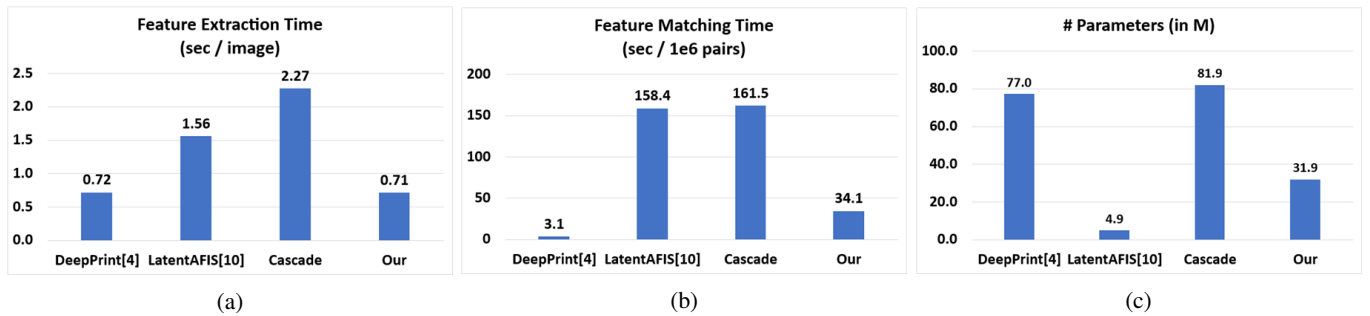


Fig. 6: Comparison of time and memory requirements with state-of-the-art methods.

$\theta_t = 0.75$ and $\theta_f = 0.15$ as this provides the best trade-off between matching time and performance as shown in Table IV.

TABLE IV: $FRR\%@FAR = 0.1\%$ for FVC 2006 DB2A[24] using various Thresholding hyperparameter values.

θ_t	θ_f	%times when $\theta_f \leq s_g \leq \theta_t$	Matching Time (sec / 1e6 pairs)	$FRR\%$
> 1	< 0	100.00	161.48	0.11
0.8	0.1	25.03	42.74	0.11
0.75	0.15	19.56	34.08	0.12
0.7	0.2	12.97	23.63	0.83

C. Score Normalization and Fusion

In Table V we set $\theta_t > 1$ and $\theta_f < 0$ so that we can explore the various score normalization and fusion techniques[20] independent of Thresholding. We again use FVC2006 DB2A[24] as a hold-out dataset to determine any hyperparameters required for normalization.

Double Sigmoid[19], being the most robust and efficient technique, gives the best performance among normalizations. Although Max-Fusion gives a better performance with Double Sigmoid[19] than Mean-Fusion, it is much more sensitive to normalization and Thresholding.

TABLE V: Average $FRR\%@FAR = 0.1\%$ over optical FVC datasets(as in Table I) w.r.t. score normalization and fusion.

Normalization	Mean-Fusion	Max-Fusion	Min-Fusion
None	2.22	2.51	5.75
Min-max	1.79	5.82	2.51
z-score	1.77	4.57	2.42
Median and MAD	1.91	2.51	3.93
Modified tanh[27]	1.77	4.57	2.42
Double Sigmoid[19]	1.68	1.46	3.70

D. Amount of Local Information

In this study we set $\theta_t > 1$ and $\theta_f < 0$ and alter the amount of local information available for fusing by controlling the number of minutiae points used for Local Matching during inference. Figure 7 clearly shows that a smaller subset leads to faster matching speeds but worse performances. This introduces

a trade-off, but it is interesting to note that the deterioration in performance of our method is significantly less as compared to [10] due to the constant advantage of fusion with global scores. Hence this approach of selecting a random minutiae subset and merging local with global scores in all cases can be used as an alternative to Thresholding to speed-up feature matching while maintaining performance.

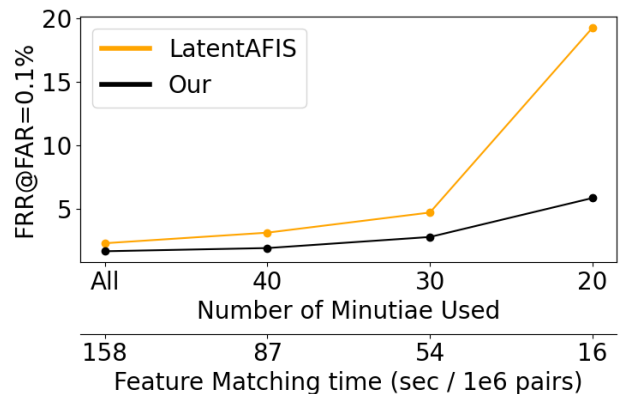


Fig. 7: Variation in average performance(as in Table I) and feature matching time with respect to number of minutiae used.

VI. CONCLUSIONS AND FUTURE WORK

We presented a novel methodology for fingerprint feature extraction where a single end-to-end transformer model can be used to parallelly and efficiently obtain global representations, minutiae predictions as well as local representations from fingerprint images instead of employing a separate module for each of them. To prove the utility of combining global and local perspectives, we also present an efficient feature matching process over these representations to achieve state-of-the-art performances on multiple datasets.

A possible future extension of this work can be incorporating a filtering mechanism for spurious minutiae (as shown in Figure 4) so that we can use different number of minutiae points for different images instead of a constant L . This is important as this eliminates false minutiae matches and any potential attacks exploiting a fixed number of local features. We are also working on merging this work with [11] to integrate spoof detection in this methodology and eliminate the vulnerability against presentations attacks.

VII. SUPPLEMENTARY: PRIVATE DATASET EXPERIMENTS

This section includes supplementary material related to the experiments performed using models trained on the in-house dataset.

A. ROC curves

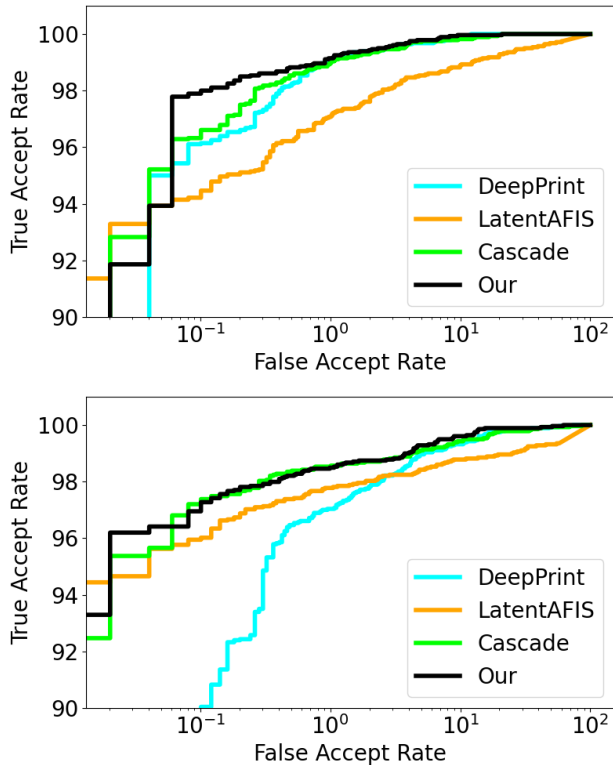


Fig. 8: ROC curves of our method, DeepPrint[4] and LatentAFIS[10] for FVC2004 DB1A and DB2A respectively.

Figure 8 shows the curves of True Accept Rate vs False Accept Rate for FVC2004[23] DB1A and DB2A. Here True Accept Rate refers to the percentage of genuine pairs predicted as genuine and False Accept Rate refers to the percentage of impostor pairs predicted as genuine. These clearly show the performance advantage of our method at various thresholds as compared to [4], [10] and Cascade.

B. Generalization examples

Figure 9 shows examples of images from the different kinds of sensors used for experimentation.

VIII. SUPPLEMENTARY: ABLATION STUDY OF NUMBER OF DECODER LAYERS

We try to alter the number of layers in f_{dec} and observe the variation in performance. Table VI clearly shows that with increasing number of decoder layers the validation losses L_{po} and L_e converge to better minimas. But with increasing number of decoder layers the model complexity increases and hence the inference time for feature extraction also increases. Our choice of using 6 layers in our main experimentation is justified as we



(a) Optical images used for training and same-sensor testing.



(b) Thermal images.



(c) Synthetic images.



(d) Capacitive images.

Fig. 9

are able to get the best model with feature extraction time per image comparable to that of [4].

IX. PUBLIC DATASET EXPERIMENTS

This section repeats the experimentation performed in the main paper, but here we train our models with public datasets. This is done to make our work accessible and reproducible.

A. Datasets

For training and validation purposes we use a combination of multiple datasets to maximize the effectiveness of the training stage. They include the plain images from NIST SD 300[28], optical images from NIST SD 302[29], MCYT[30] and live images from LivDet 2011[31], 2013[32], 2015[33] and 2017[34]. This gives us a huge dataset that spans multiple sources and years. The details of each of the aforementioned datasets can be found in Table VII.

TABLE VI: Variation in validation losses and inference time with respect to the number of layers in the decoder.

# Decoder Layers	$L_{po} \times 10^{-3}$	$L_e \times 10^{-3}$	CPU Inference Time (sec)
1	5.77	4.00	0.660
2	5.31	3.92	0.674
3	5.07	3.86	0.681
4	4.88	3.75	0.690
5	4.78	3.70	0.697
6	4.69	3.65	0.709

For testing we use the same datasets and procedures as described in the main paper.

TABLE VII: Details of the training and validation dataset.

Name	# train images	# val images
NIST SD 300 [28]	6927	1763
NIST SD 302 [29]	5332	1304
MCYT [30]	19199	4800
LivDet [31], [32], [33], [34]	13749	15118
Total	~ 45K	~ 23K

B. Results

Table VIII presents the results obtained by our approach when trained using the public datasets. Since this dataset is smaller than the in-house data we observe some drop in performance, but we are still much better than the [4] and [10] baselines. As compared to Cascade, we still retain all the time and memory advantages discussed in the main paper.

X. SUPPLEMENTARY: IMPLEMENTATION DETAILS

We preprocess the images by segmenting them, followed by a center crop / padding to size 441×441 , a resize to size 410×410 and another center crop of size 384×384 . The coordinates and orientation of the minutiae points are altered accordingly. This procedure is similar to the one followed in [4].

All experimentation was performed using the PyTorch framework and two Nvidia 2080-Ti GPUs. An Intel(R) Xeon(R) CPU E5-2640 v4 @ 2.40GHz was used for inference purposes. A batch size of 32 was used to train all models along with an adamW[35] optimizer and cosine learning rate schedule of 100 epochs initialised with $1e^{-4}$. The value of L was set to 50 based on the average number of minutiae in the training set. We set $d_{enc} = d_{dec} = 384$ and based on the ground truth the values for d_g and d_m were set to 192 and 64 respectively.

REFERENCES

- [1] A. K. Jain, S. Prabhakar, L. Hong, and S. Pankanti, "Fingercode: A filterbank for fingerprint representation and matching," in *1999 Conference on Computer Vision and Pattern Recognition (CVPR '99)*, 23-25 June 1999, Ft. Collins, CO, USA. IEEE Computer Society, 1999, p. 2187. [Online]. Available: <https://doi.org/10.1109/CVPR.1999.784628>
- [2] K. Cao and A. K. Jain, "Fingerprint indexing and matching: An integrated approach," in *2017 IEEE International Joint Conference on Biometrics, IJCB 2017, Denver, CO, USA, October 1-4, 2017*. IEEE, 2017, pp. 437–445. [Online]. Available: <https://doi.org/10.1109/BTAS.2017.8272728>
- [3] D. Song and J. Feng, "Fingerprint indexing based on pyramid deep convolutional feature," in *2017 IEEE International Joint Conference on Biometrics (IJCB)*, 2017, pp. 200–207.
- [4] J. J. Engelsma, K. Cao, and A. K. Jain, "Learning a fixed-length fingerprint representation," *IEEE Trans. Pattern Anal. Mach. Intell.*, vol. 43, no. 6, pp. 1981–1997, 2021. [Online]. Available: <https://doi.org/10.1109/TPAMI.2019.2961349>
- [5] S. Yoon and A. Jain, "Longitudinal study of fingerprint recognition," *Proceedings of the National Academy of Sciences of the United States of America*, vol. 112, 06 2015.
- [6] S. Pankanti, S. Prabhakar, and A. Jain, "On the individuality of fingerprints," *IEEE Transactions on Pattern Analysis and Machine Intelligence*, vol. 24, no. 8, pp. 1010–1025, 2002.
- [7] R. Cappelli, M. Ferrara, and D. Maltoni, "Minutia cylinder-code: A new representation and matching technique for fingerprint recognition," *IEEE Transactions on Pattern Analysis and Machine Intelligence*, vol. 32, no. 12, pp. 2128–2141, 2010.
- [8] D. Song, Y. Tang, and J. Feng, "Aggregating minutia-centred deep convolutional features for fingerprint indexing," *Pattern Recognition*, vol. 88, pp. 397–408, 2019. [Online]. Available: <https://www.sciencedirect.com/science/article/pii/S0031320318304072>
- [9] R. Li, D. Song, Y. Liu, and J. Feng, "Learning global fingerprint features by training a fully convolutional network with local patches," *2019 International Conference on Biometrics (ICB)*, pp. 1–8, 2019.
- [10] K. Cao, D. Nguyen, C. Tymoszek, and A. K. Jain, "End-to-end latent fingerprint search," *IEEE Trans. Inf. Forensics Secur.*, vol. 15, pp. 880–894, 2020. [Online]. Available: <https://doi.org/10.1109/TIFS.2019.2930487>
- [11] A. Popli, S. Tandon, J. J. Engelsma, N. Onoe, A. Okubo, and A. Namboodiri, "A unified model for fingerprint authentication and presentation attack detection," 2021.
- [12] A. Dosovitskiy, L. Beyer, A. Kolesnikov, D. Weissenborn, X. Zhai, T. Unterthiner, M. Dehghani, M. Minderer, G. Heigold, S. Gelly, J. Uszkoreit, and N. Houlsby, "An image is worth 16x16 words: Transformers for image recognition at scale," in *International Conference on Learning Representations*, 2021. [Online]. Available: <https://openreview.net/forum?id=YicbFdNTTy>
- [13] N. Carion, F. Massa, G. Synnaeve, N. Usunier, A. Kirillov, and S. Zagoruyko, "End-to-end object detection with transformers," in *Computer Vision – ECCV 2020*, A. Vedaldi, H. Bischof, T. Brox, and J.-M. Frahm, Eds. Cham: Springer International Publishing, 2020, pp. 213–229.
- [14] S. B. Sandouka, Y. Bazi, and N. Alajlan, "Transformers and generative adversarial networks for liveness detection in multitarget fingerprint sensors," *Sensors*, vol. 21, no. 3, 2021. [Online]. Available: <https://www.mdpi.com/1424-8220/21/3/699>
- [15] H. Wu, B. Xiao, N. Codella, M. Liu, X. Dai, L. Yuan, and L. Zhang, "Cvt: Introducing convolutions to vision transformers," *arXiv preprint arXiv:2103.15808*, 2021.
- [16] S. A. A. Ahmed, M. Awais, and J. Kittler, "Sit: Self-supervised vision transformer," *ArXiv*, vol. abs/2104.03602, 2021.
- [17] J. He, J. Chen, S. Liu, A. Kortylewski, C. Yang, Y. Bai, C. Wang, and A. L. Yuille, "Transfg: A transformer architecture for fine-grained recognition," *ArXiv*, vol. abs/2103.07976, 2021.
- [18] H. W. Kuhn and B. Yaw, "The hungarian method for the assignment problem," *Naval Res. Logist. Quart.*, pp. 83–97, 1955.
- [19] R. Cappelli, D. Maio, and D. Maltoni, "Combining fingerprint classifiers," in *Proceedings of the First International Workshop on Multiple Classifier Systems*, ser. MCS '00. Berlin, Heidelberg: Springer-Verlag, 2000, p. 351–361.
- [20] A. Jain, K. Nandakumar, and A. Ross, "Score normalization in multimodal biometric systems," *Pattern Recognition*, vol. 38, no. 12, pp. 2270–2285, 2005. [Online]. Available: <https://www.sciencedirect.com/science/article/pii/S0031320305000592>

TABLE VIII: Comparison of the matching performance ($FRR\%@FAR = 1.0\%$) on FVC datasets' optical sensors

Method	2006	2004		2002		2000		Average [†]
	DB2A	DB1A	DB2A	DB1A	DB2A	DB1A	DB3A	
DeepPrint [4]	0.12	0.96	2.96	4.11	1.82	1.79	2.04	2.28
LatentAFIS [10]	0.00	2.89	2.22	0.54	0.25	0.68	1.25	1.31
Cascade	0.00	0.96	1.44	0.43	0.21	0.25	0.43	0.62
Our Public ($\theta_t = 0.75$ and $\theta_f = 0.15$)	0.08	1.21	1.61	0.75	0.93	0.39	0.50	0.90

[†] FVC 2006 DB2A has not been included in the average.

- [21] D. Maio, D. Maltoni, R. Cappelli, J. L. Wayman, and A. K. Jain, "Fvc2000: fingerprint verification competition," *IEEE on Pattern Analysis and Machine Intelligence*, 2002.
- [22] D. Maio, D. Maltoni, R. Cappelli, J. L. Wayman, and A. K. Jain, "Fvc2002: Second fingerprint verification competition," in *Object recognition supported by user interaction for service robots*, 2002.
- [23] D. Maio, D. Maltoni, R. Cappelli, J. L. Wayman, and A. K. Jain, "Fvc2004: Third fingerprint verification competition," in *Biometric Authentication*, D. Zhang and A. K. Jain, Eds. Springer Berlin Heidelberg, 2004, pp. 1–7.
- [24] R. Cappelli, M. Ferrara, A. Franco, and D. Maltoni, "Fingerprint verification competition 2006," *Biometric Technology Today*, vol. 15, no. 7, pp. 7 – 9, 2007. [Online]. Available: <http://www.sciencedirect.com/science/article/pii/S0969476507701406>
- [25] T. Chugh, S. S. Arora, A. K. Jain, and N. G. Paulter, "Benchmarking fingerprint minutiae extractors," in *2017 International Conference of the Biometrics Special Interest Group (BIOSIG)*, 2017, pp. 1–8.
- [26] K. Ko, "User's guide to nist biometric image software (nbis)," 2007-01-21 2007.
- [27] L. Latha and S. Thangasamy, "Efficient approach to normalization of multimodal biometric scores," 2011.
- [28] G. Fiumara, P. Flanagan, J. Grantham, B. Bandini, K. Ko, and J. Libert, "National institute of standards and technology special database 300:uncompressed plain and rolled images from fingerprint cards," National Institute of Standards and Technology, Technical Note 1993, Jun. 2018.
- [29] G. Fiumara, P. Flanagan, J. Grantham, K. Ko, K. Marshall, M. Schwarz, E. Tabassi, B. Woodgate, and C. Boehnen, "Nist special database 302: Nail to nail fingerprint challenge," 2019-12-11 2019.
- [30] J. Ortega-Garcia, "Mcyt baseline corpus: a bimodal biometric database," *IEE Proceedings - Vision, Image and Signal Processing*, vol. 150, pp. 395–401(6), December 2003. [Online]. Available: https://digital-library.theiet.org/content/journals/10.1049/ip-vis_20031078
- [31] D. Yambay, L. Ghiani, P. Denti, G. L. Marcialis, F. Roli, and S. Schuckers, "Livdet 2011 — fingerprint liveness detection competition 2011," in *2012 5th IAPR International Conference on Biometrics (ICB)*, 2012, pp. 208–215.
- [32] L. Ghiani, D. Yambay, V. Mura, S. Tocco, G. L. Marcialis, F. Roli, and S. Schuckers, "Livdet 2013 fingerprint liveness detection competition 2013," in *2013 International Conference on Biometrics (ICB)*, 2013, pp. 1–6.
- [33] V. Mura, L. Ghiani, G. L. Marcialis, F. Roli, D. A. Yambay, and S. A. Schuckers, "Livdet 2015 fingerprint liveness detection competition 2015," in *2015 IEEE 7th International Conference on Biometrics Theory, Applications and Systems (BTAS)*, 2015, pp. 1–6.
- [34] D. Yambay, S. Schuckers, S. Denning, C. Sandmann, A. Bachurinski, and J. Hogan, "Livdet 2017 - fingerprint systems liveness detection competition," in *2018 IEEE 9th International Conference on Biometrics Theory, Applications and Systems (BTAS)*, 2018, pp. 1–9.
- [35] I. Loshchilov and F. Hutter, "Decoupled weight decay regularization," in *International Conference on Learning Representations*, 2019. [Online]. Available: <https://openreview.net/forum?id=Bkg6RiCqY7>